Chaos, Solitons and Fractals 95 (2017) 52–56

Contents lists available at ScienceDirect

Chaos, Solitons and Fractals

Nonlinear Science, and Nonequilibrium and Complex Phenomena

journal homepage: www.elsevier.com/locate/chaos

Nature of electrical transport properties of nanocrystalline $ZnIn_2Se_4$ thin films

M.M. El-Nahass, A.A. Attia, H.A.M. Ali*, G.F. Salem, M.I. Ismail

Physics Department, Faculty of Education, Ain Shams University, Roxy, Cairo, 11757, Egypt

ARTICLE INFO

Article history:
Received 8 July 2016
Revised 12 December 2016
Accepted 12 December 2016

Keywords:
$ZnIn_2Se_4$ thin films
Atomic force microscope
Electrical transport properties
Conduction mechanisms

ABSTRACT

$ZnIn_2Se_4$ thin films were deposited on glass substrates by thermal evaporation technique. Some of $ZnIn_2Se_4$ films were annealed under vacuum at 623 K for 2 h. Atomic force microscope (AFM) images were analyzed for as-deposited and annealed films. The roughness degree of the film surface decreased under the influence of annealing. DC Electrical conductivity studied as a function of temperature. Two activation energies were determined that $\Delta E_1 = 0.44$ eV and $\Delta E_2 = 0.65$ eV. Using thermo-electric measurements, the thermoelectric power factor (P), carrier concentration (n) and mobility (μ) were calculated. Current density–voltage characteristics of Al/$ZnIn_2Se_4$/Al sandwich structure were examined. Different mechanisms were obtained; ohmic conduction mechanism at lower voltages and space charge limited conductivity (SCLC) mechanisms at higher voltages.

1. Introduction

Zinc Indium Selenide ($ZnIn_2Se_4$) is a ternary chalcogenide semiconductor of type $A^{II}B_2^{III}X_4^{VI}$, where A=Zn, Cd or Hg, B=Al, In or Ga, and X=Se, S or Te [1,2]. Ternary semiconducting compounds have been generally researched as a result of their potential applications in the electro-optic, optoelectronic, and nonlinear optical devices. [3]. These compounds are majority crystallized in a tetragonal structure [4]. Consequently, there is much interest in the preparation and characterization of chalcogenide thin films [5]. Thin films of $ZnIn_2Se_4$ have been grown using different techniques such as spray pyrolysis technique [5], flash evaporation technique [4], chemical bath deposition [6,7] and thermal evaporation [8]. $ZnIn_2Se_4$ thin films have wide applications in solar cells and optoelectronic devices [5], as a memory switching device [9] and in photo-detector device [10]. Likewise, it utilized as the novel buffer layer in place of toxic CdS and demonstrates a cell efficiency of 15.3% in the fabrication of Cu(In,Ga)Se_2 based-solar cells [7,11]. The interface between $ZnIn_2Se_4$ and Cu(In,Ga)Se_2 produces a depletion region which facilitates the formation of the p–n junction. However, the incorporation of Zn ions into Cu(In,Ga)Se_2 films is difficult to control, and the excess dopants cause the formation of the impurities [12]. Some studies analyzed the dopant concentration in heterostructure and found that increasing the difference between diffusion coefficients of layers of heterostructure leads to increase the homogeneity of impurities in doped region [13].

The physical properties that underpin the operation of electronic devices depend on chemical bonding and crystalline nature of the materials [14]. There are many characterization's tools that can provide a useful insight into the mechanisms of the charge transport through films of materials. Analyses of electron transport parameters are promising methods based on the measurements of device I–V characteristics, I–V characteristic nonlinearity [15] and electronic noise characteristics [16–20]. In the present work, thin films of $ZnIn_2Se_4$ were prepared by thermal evaporation method and deposited onto glass substrates. A detailed experimental study carried out on the structural and electrical transport properties of $ZnIn_2Se_4$ films as a function of temperature: in particular, Atomic force microscope, electrical conductivity, thermoelectric power and J–V characteristics.

2. Experimental technique

The ingots of Zinc Indium Selenide were prepared by fusion of stoichiometric quantities of pure elements in vacuum sealed silica tubes. They were left at 1323 K for 10 h and then cooled to room temperature over 48 h. Thin films with different thicknesses were prepared by the thermal evaporation technique under a vacuum of about 10^{-4} Pa using coating unit (Edwards type E306A, England). The deposition rate was controlled at 2.5 nm s^{-1}. The film thickness was calculated using a quartz crystal thickness monitor (FTM4, Edwards) and then it was checked by the Tolansky's interferometric technique [21]. The film depositions were made at room temperature. Some films were annealed under vacuum at 623 K for 2 h. The 2D and 3D images of the morphology of film sur-

* Corresponding author .
E-mail address: hend2061@yahoo.com (H.A.M. Ali).

http://dx.doi.org/10.1016/j.chaos.2016.12.005
0960-0779/

face were examined utilizing atomic force microscopy technique, model (Wet-SPM Shimadzu). The particles mean radius and surface roughness of $ZnIn_2Se_4$ thin films were calculated by using computer programming. The DC electrical measurements were carried out using two probe method for a planar sample. The ohmic electrodes at the two ends of the thin films were made by thermal evaporation of Al. The electrical resistivity of films was measured by a high internal impedance electrometer (Keithely 617A). Then, the DC conductivity (σ_{DC}) was calculated from the well-known relation $\sigma_{DC} = L/RA$, where L is the length of the film, R is electrical resistance and A is the cross section area of the sample. For the thermoelectric power measurements, Al electrodes were deposited into the two ends of the planer $ZnIn_2Se_4$ films. The thermoelectric power (s) was detected by measuring the voltage for a temperature gradient of 10 K over the samples using a programmable electrometer. The current density–voltage (J–V) characteristics for a sandwich sample, that has Al/$ZnIn_2Se_4$/Al structure, were measured utilizing the high impedance electrometer (Keithley 617A) as a current source and ammeter. The sample temperature measured using a chromel–alumel thermocouple appended to a digital thermometer.

3. Results and discussion

3.1. Structural topography

In our previous paper [8], we studied the structural properties of $ZnIn_2Se_4$ thin films using X-ray diffraction technique. The deposited films at room temperature showed nanocrystalline nature with crystallite size of about a few nanometers.

The knowledge of the surface topography can be obtained using atomic force microscopy (AFM) technique, which gives an excellent tool to study morphology and texture of diverse surfaces [22]. In the present work, the surface morphology for the as-deposited film of $ZnIn_2Se_4$ with thickness 473 nm and the annealed one under vacuum at 623 K for 2 h were analyzed using atomic force microscope (AFM) technique. Fig. 1(a, b) shows the 2D and 3D images of AFM for as-deposited and annealed films, respectively. The average roughness is found to decrease from 1.41 nm for the as-deposited $ZnIn_2Se_4$ film to 1.20 nm for the annealed $ZnIn_2Se_4$ film. Thus, under the influence of annealing the film provides a homogenous nature. The mean radius of particles in $ZnIn_2Se_4$ film decreased from 70 nm in the as-deposited film to 20 nm for the annealed one as observed in Fig. 1.

3.2. Electrical conductivity

3.2.1. DC electrical conductivity

Fig. 2 shows the temperature dependence of DC electrical conductivity (σ_{DC}) of $ZnIn_2Se_4$ films with thickness 371 nm. It is clear from that σ_{DC} increases with increasing temperature. Thus, DC conductivity obeys the Arrhenius relation indicating a semiconducting transport behavior [23]. The curve of σ_{DC} reveals two distinct linear regions. This result refers to the existence of two transport mechanisms, which gives two activation energies ΔE_1 and ΔE_2 for the conduction of free charge carriers. The activation energies are calculated using the following relation [24,25]:

$$\sigma_{DC} = \sigma_o e^{\frac{-\Delta E}{kT}} \tag{1}$$

where σ_o is the pre-exponential constant, k is the Boltzmann's constant, T is the absolute temperature and ΔE is the activation energy for a certain region. At lower range of temperature (293–312 K), the value of ΔE_1 is found to be 0.44 eV. ΔE_1 is attributed to the extrinsic conduction mechanism. At higher range of temperature (~312–370 K), the value of ΔE_2 is found to be 0.65 eV. ΔE_2 is ascribed to the intrinsic conduction mechanism. The value of ΔE_2 is approximately about half the onset energy gap obtained from optical measurements [8].

3.2.2. Thermoelectric power measurement

The Seebeck coefficient, S, for $ZnIn_2Se_4$ film with thickness 371 nm is measured as a function of temperature from 303 K to 350 K. It determined using the following relation [26]:

$$S = \frac{\Delta V}{\Delta T} \tag{2}$$

where ΔV is the thermo-emf produced across the sample due to the temperature difference ΔT. The variation of Seebeck coefficient as a function of temperature is shown in Fig. 3. From the figure, Seebeck coefficient is observed to be negative affirming to the n-type polarity for $ZnIn_2Se_4$ film. Thus, the most predominant carriers are electrons. Also, Seebeck coefficient increases with increasing temperature in the investigated range of temperature. In the extrinsic region ($T < 312$ K), a sharp increase in Seebeck coefficient is owing to the increasing number of thermally excited carriers [27]. Fig. 4 demonstrates the variation for both of S and $\ln \sigma_{DC}$ against the reciprocal of temperature in the intrinsic region of conduction ($T > 312$ K). In this region, the moderate increase in Seebeck coefficient may be due to the generation of the electrons from the valence band to the conduction band [28].

For assessing the potential of a thermoelectric material, it is often to use the thermoelectric power factor (P). It is evaluated from the values of DC electrical conductivity and Seebeck coefficient as [29–31]:

$$P = S^2 \sigma_{DC} \tag{3}$$

The P value is about 0.14 μW/m K^2 at 305 K. Also, the thermo electric power measurement is used to evaluate the carrier mobility (μ) and carrier concentration. The free carrier concentration, n, is determined as a function of temperature according the following equation [32,33]:

$$n = 2\left(\frac{2\pi m^* kT}{h^2}\right)^{3/2} e^{(2k-qS)/k} \tag{4}$$

where h is a Planck's constant, m^* is the effective mass that is taken as $0.15m_o$ [34], q is the electronic charge and k is in eV/K. Using the values of S, the value of n is calculated. The value of n increases with increasing temperature in the range of 1.1–1.4 × 10^{25} m^{-3} which corresponding to the temperature range of 300–360 K.

The mobility (μ) of the charge carriers is determined from the relations [25,35]:

$$\mu = \frac{\sigma_{DC}}{nq}, \quad \mu = \mu_o e^{\left(\frac{-\Delta E_\mu}{kT}\right)} \tag{5}$$

where μ_o is the grain boundary limited mobility and ΔE_μ is the mobility activation energy. Fig. 5 represents the temperature dependence of the charge carriers mobility. As observed μ values increase with increasing temperature. The activation energy for the mobility is determined by plotting $\ln \mu$ against $1000/T$ as seen in the inset of Fig. 5. The calculated values of μ_o and ΔE_μ are 2.91 × 10^{-3} m^{2}V^{-1}S^{-1} and 0.49 eV, respectively.

3.2.3. Current density–voltage (J–V) characteristics

J-V characteristics are taken at constant temperature (293, 303, 308, 313 K) for Al/$ZnIn_2Se_4$/Al sandwich structure of a sample deposited on glass substrate. The configuration of the sample design is shown in Fig. 6. Fig. 7 represents a typical log J-log V characteristics for Al/$ZnIn_2Se_4$/Al at different temperatures. The current density increases with the increase in the applied voltage and temperature. The graphs for J-V characteristics reveal three distinct regions with different slopes (m) for each temperature, where $J \alpha V^m$.

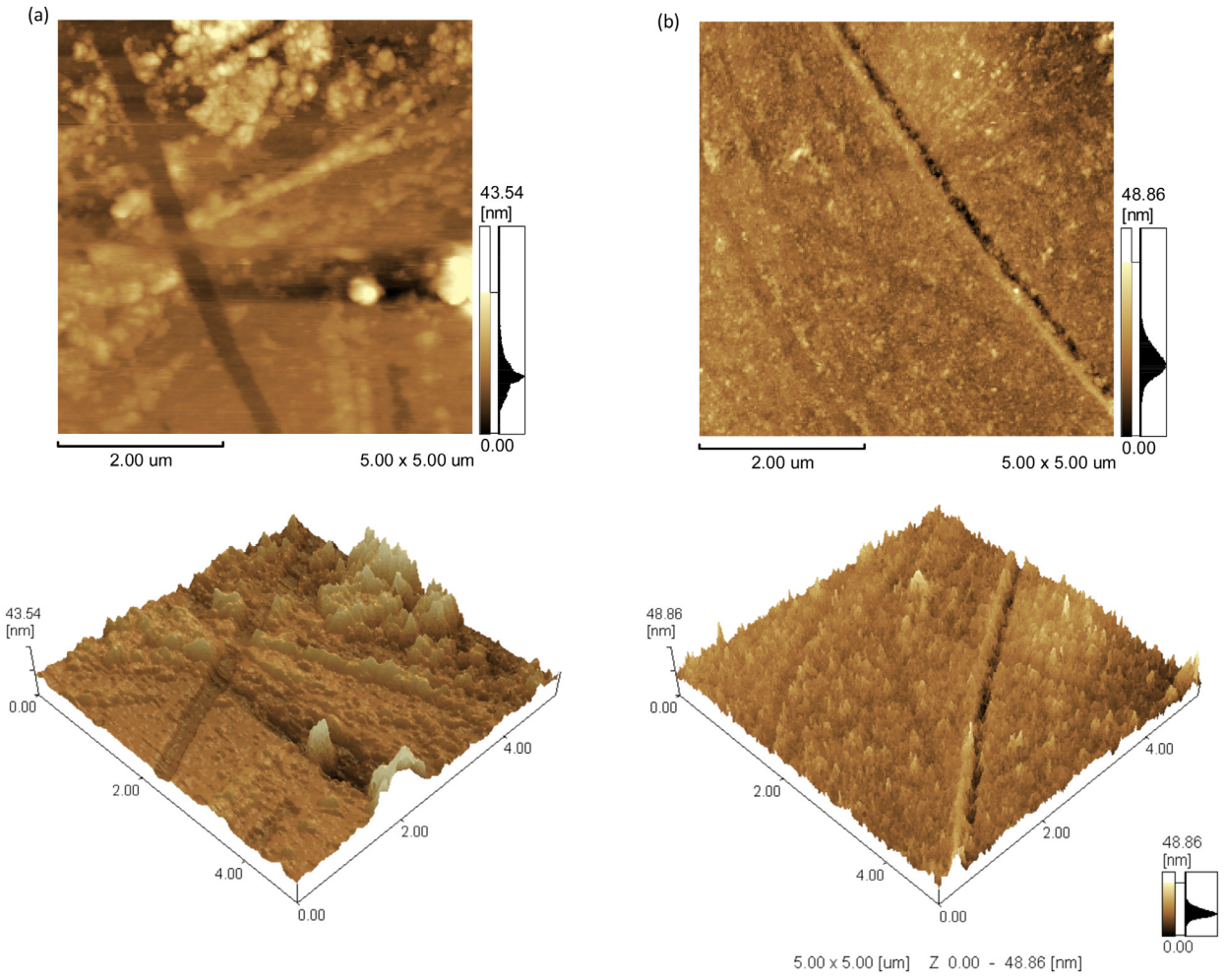

Fig. 1. 2D and 3D images of AFM (a,b) for as-deposited and annealed films of $ZnIn_2Se_4$, respecteively.

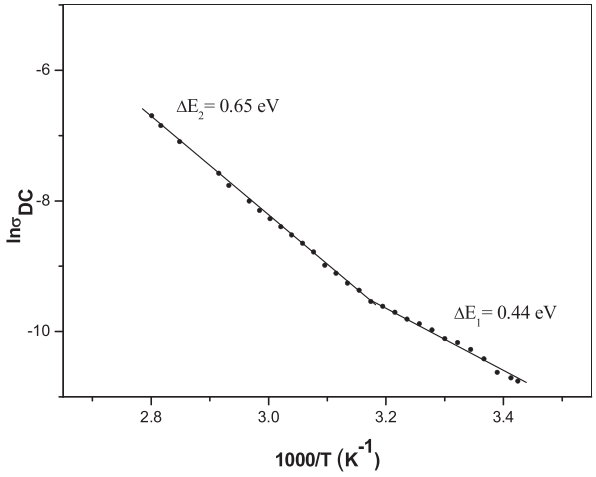

Fig. 2. Temperature dependence of DC electrical conductivity (σ_{DC}) of $ZnIn_2Se_4$ thin film.

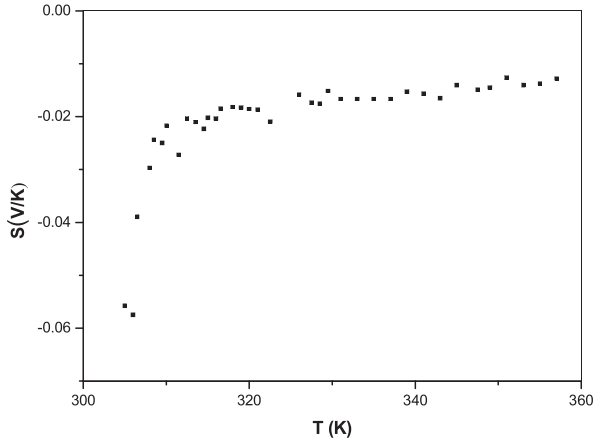

Fig. 3. Seebeck coefficient (S) of $ZnIn_2Se_4$ thin film as a function of temperature.

From the analysis, the logarithmic slope (m) of these regions (i, ii, iii) are 1, 2, >2, respectively. Thus, there are three different types of conduction mechanisms. Region i of J–V is corresponding to ohmic region, where the conductivity is described by [36,37]:

$$J = \frac{n_o q \mu V}{d} \quad (6)$$

where n_o the concentration of thermally– generated electrons in the conduction band, V the applied voltage and d is the film thickness (473 nm). The ohmic region is separated by a well-defined cross-over voltage (V_x) from the second region ii, in which the logarithmic slope of J–V is 2. This voltage is at which the current-voltage characteristics transits from ohm's law to the trap-free square law. The obtained values of V_x decreased with the increase in temperature as seen in Table 1. In region ii of J–V ($J \alpha V^2$),

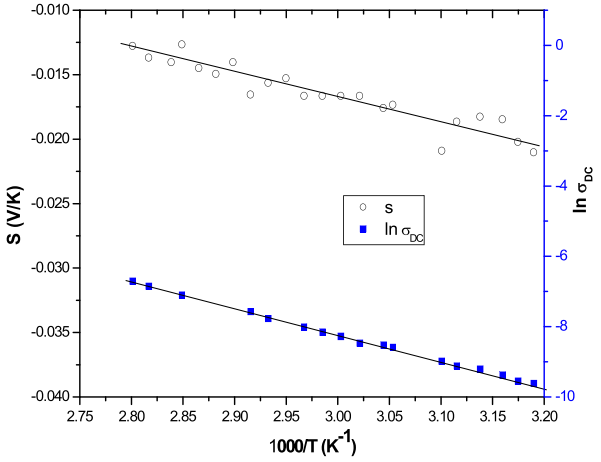

Fig. 4. The variation of Seebeck coefficient (S) and DC electrical conductivity (σ_{DC}) against 1000/T.

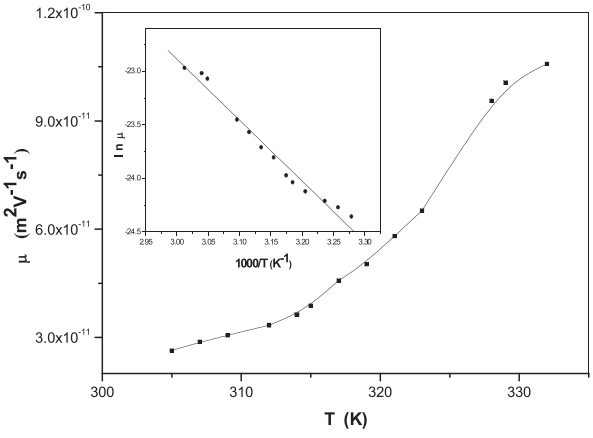

Fig. 5. Temperature dependence of mobility (μ) of $ZnIn_2Se_4$ thin film.; inset Fig.: Plot of ln μ against 1000/T.

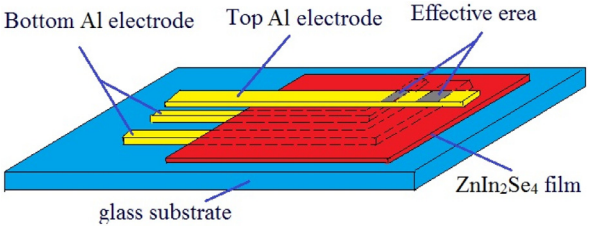

Fig. 6. The configuration of Al/ $ZnIn_2Se_4$/Al structure.

Table 1
The values of V_x, V_{TR}, V_{TFL}, N_t and N_c of $ZnIn_2Se_4$ thin film at different temperatures.

T (K)	V_x(volts)	V_{TR}(volts)	V_{TFL}(volts)	$N_t(10^{22}\ m^{-3})$	$N_C(10^{39}\ m^{-3})$
298	2.5	4.15	4.5	1.8	4.80
303	1.95	2.99	3.35	1.34	3.57
308	1.4	2.1	2.5	1.0	2.67
313	1	1.5	1.55	0.62	1.65

the current density follows a square-law voltage dependence. The conduction mechanism in this region is referred to space charge limited current (SCLC) mechanism controlled by a single discrete trapping level and it is expressed by Mott–Gurney square law

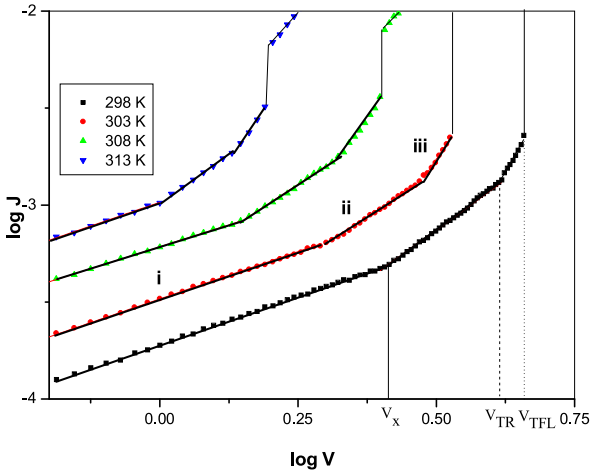

Fig. 7. J–V characteristics of Al/ $ZnIn_2Se_4$/Al at different temperatures.

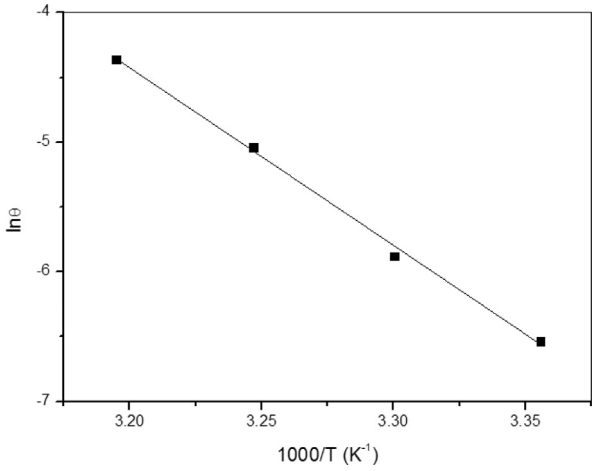

Fig. 8. Plot of ln θ against 1000/T.

[38,39] as:

$$J = \frac{9}{8}\varepsilon\mu\theta\frac{V^2}{d^3} \tag{7}$$

where ε is the permittivity of the material (7.154×10^{-11} Fm^{-1} [8]) and θ is the ratio of free-to-trapped electron concentration and is given by [36]:

$$\theta = \frac{N_c}{gN_t}e^{\frac{-E_t}{kT}} \tag{8}$$

where N_C is the effective density of states in the conduction band, g is the degeneracy factor for the traps, N_t is the concentration of traps situated at an energy E_t below the conduction band edge. The values of θ are determined from the intercept of the straight lines of log J - log V at different temperatures. Fig. 8 shows the relation between ln θ against 1000/T. From the slope of the linear line, the value of E_t is found to be 1.18 eV. The value of N_t is calculated depending on the trap-filled-limited voltage (V_{TFL}) value using the following equation:

$$N_t = \frac{2\varepsilon V_{TFL}}{qd^2} \tag{9}$$

At the trap-filled-limit (TFL) voltage or at V_{TFL}, the entire population of traps has been filled, and the current rises nearly vertically. The value of N_t is found to be of the order of 0.62–1.80×10^{22} m^{-3} for the temperature range of 298–313 K as seen in Table 1. The effective density of states in the conduction band

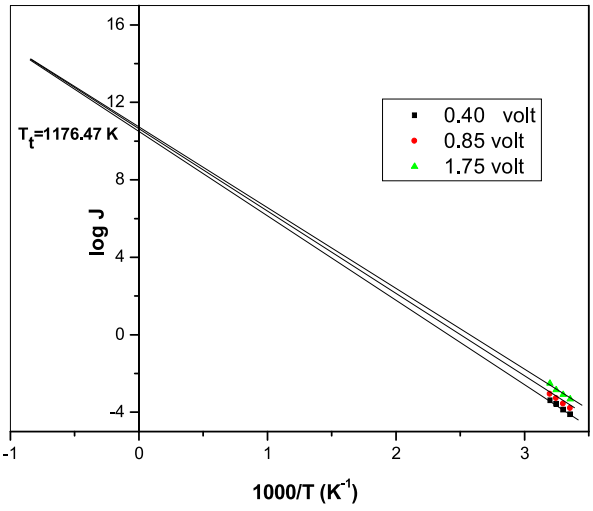

Fig. 9. Temperature dependence of current density J for Al/ $ZnIn_2Se_4$/Al at different voltages.

(N_C) is determined by substituting the value of N_t in the intercept of the fitting line in Fig. 8 and g value is taken as 2 for electron traps. Then, the value of N_C is found to be in the range of 1.65–4.80 × 10^{39} m^{-3} for the investigated range of temperature as also shown in Table 1. Moreover, the transition voltage (V_{TR}) from region ii to region iii is obtained at different temperatures and listed in Table 1. The transition voltage decreased with the increase in temperature. Finally, region iii of slope m (~4.93) is related to space charge limited current (SCLC) region mechanism with an exponential distribution of traps. The SCLC mechanism and non-ohmic behavior are explained in terms of trap controlled space charge limited conduction [40]. The defects in the materials work as trapping centers which become filled by the injected charge carriers from the electrode, happened to be charged and build up a space charge which leads to the SCLC process [41–42].

The current density is described by [43,44]:

$$J = q\mu N_c \left(\frac{\varepsilon}{qN_o kT_t}\right)^l \frac{V^{l+1}}{d^{2l+1}} \quad (10)$$

where $N_\circ$ is the trap density per unit energy range at the conduction band edge, and l ($l = m - 1$) is the ratio T_t / T, where T is the absolute temperature and T_t is temperature parameter characterizing trap distribution. Fig. 9 illustrates the temperature dependence of current density in region iii at different voltages. Linear lines are obtained and upon extrapolating the lines in the direction of ordinate axis, it interacts at a common point corresponding to |1 / T_t | on the abscissa axis [43]. The obtained value of T_t is ≈1176 K, which is consistent with that obtained from the value of l (1171.63 K).

4. Conclusion

Zinc Indium Selenide ($ZnIn_2Se_4$) thin films were thermally prepared onto glass substrates at room temperature. The surface morphology studies by AFM technique demonstrated that the annealed film of $ZnIn_2Se_4$ at 623 K for 2 h under vacuum has a homogenous nature with smaller roughness than the as-deposited film. DC electrical conductivity of $ZnIn_2Se_4$ film showed a semiconductor behavior with two types of conduction mechanisms; $\Delta E_1 = 0.44$ eV and $\Delta E_2 = 0.65$ eV. The thermoelectric measurements showed a n-type polarity of $ZnIn_2Se_4$ thin films. The Seebeck coefficient of $ZnIn_2Se_4$ film increased with the increase in temperature. The value of thermoelectric power factor is about 0.14 μ W/m K^2 at 305 K. The carrier concentration value is in order of 10^{25} m^{-3}. It increases with the increase in temperature. The mobility activation energy was calculated to be 0.49 eV. The characteristics (J–V) for Al/$ZnIn_2Se_4$/Al structure revealed three distinct regions. The current transport mechanisms are varied from ohmic conduction to space charge limited conduction with single trap level to space charge limited conduction accompanied by an exponential distribution of traps, respectively. The trap-filled-limited voltage (V_{TFL}) was found to decrease with increasing temperature. The temperature parameter that is characterized the exponential trap distribution (T_t) is ≈1176 K.

References

[1] Cheng KW, Huang CM, Yu YC, Li CT, Shu CK, Liu WL. Sol Energy Mater Sol Cells 2011;95:1940.
[2] Yadava SP, Shinde PS, Rajpure KY, Bhosale CH. Sol Energy Mater Sol Cells 2008;92:453.
[3] Ozaki S, Muto KI, Nagata H, Adachi S. J Appl Phys 2005;97:043507.
[4] Dhruv DK, Patel BH. Int J Appl Sci Eng Res 2014;1:121.
[5] Yadav SP, Shinde PS, Rajpure KY, Bhosale CH. J Phys Chem Solids 2008;69:1747.
[6] Babu P, Ramakrishna Reddy KT, Miles RW. Energy Procedia 2011;10:177.
[7] Babu P, Reddy MRV, Reddy KTR. Electron Mater Lett 2014;10(4):731.
[8] El-Nahass MM, Attia AA, salem GF, Ali HAM, Ismail MI. Physica B 2013;425:23.
[9] Dhruv DK, Nowicki A, Patel BH, Dhamecha VD. Surface Engineering 2015;31(7):556.
[10] Mandal L, Chaudhari NS, Ogale S. ACS Appl Mater Interfaces 2013;5:9141.
[11] Babu P, Ramakrishna Reddy KT, Miles RW. Energy Procedia 2011;10:177.
[12] Lin SH, Lu CH. J Mater Sci 2014;25:3622.
[13] Pankratov EL, Spagnolo B. Eur Phys J B 2005;46:15.
[14] Petty MC. Molecular electronics: from principles to practice. Chichester, UK: Wiley; 2007.
[15] Sita Z, Sedlakova V, Majzner J, Sedlak P, Sikula J, Grmela L. Metrol Meas Syst 2013;XX(4):635.
[16] Jamal Deen M, Rumyantsev SL, Landheer D, Xu D-X. Appl Phys Lett 2000;77:2234.
[17] Fantini P, Pirovano A, Ventrice D. A Redaelli Appl Phys Lett 2006;88:263506.
[18] Lanzara E, Mantegna RN, Spagnolo B, Zanagara R. Am J Phys 1997;65:341.
[19] Klyuev AV, Yakimov AV. Physica B 2014;440:145.
[20] Kumar A, Nagarajan S, Sopanen M, Kumar V, Singh R. Semicond Sci Technol 2015;30:105022.
[21] Tolansky S. Multiple beam interference microscopy of metals. London: Academic Press; 1970. p. 55.
[22] KUMARa BR, RAO TS. Dig J Nanomater Biostruct 2012;7:1881.
[23] Patil V, Pawar S, Chougule M, Godse P, Sakhare R, Sen S, et al. J Surf Eng Mater Adv Technol 2011;1:35.
[24] Dwivedi DK, Ashankar D, Dubey M. Rom J Phys 2010;55(3–4):352.
[25] Braunger ML, Escanhoela CA Jr, Fier I, Walmsley L, Ziemath EC. J Non-Cry Solids 2012;358:2855.
[26] Ravinder D. Mater Lett 2000;44:130.
[27] Batal MA, Nashed G, Jneed FH. J Assoc Arab Univ Basic Appl Sci 2014;15:15.
[28] Soliman LI, Nassary MM, Shaban HT, Salwa AS. Vacuum 2010;85(3):358.
[29] Zide JM, Klenov DO, Stemmer S, Gossard AC, Zeng G, Bowers JE, et al. Appl Phys Lett 2005;87:112102.
[30] Kerdsongpanya S, Nong NV, Pryds N, Z˙ukauskaite A, Jensen J, Birch J, et al. Appl Phys Lett 2011;99:232113.
[31] Rivas-Murias B, Muguerra H, Traianidis M, Henrist C, Vertruyen B, Cloots R. Sol Stat Sci 2010;12:1490.
[32] Atyia HE, El-Barry AMA. Chalcogenide Lett 2006;3:41.
[33] Khan ZH, Zulfequar M, Ilyas M, Husain M. Acta Phys Pol A 2000;98:93.
[34] Setyawan W, Gaume RM, Lam S, Feigelson RS, Curtarolo S. ACS Comb Sci 2011;13:382.
[35] Patil V, Joshi P, Chougule M, Sen S. Soft Nanosci Lett 2012;2:1.
[36] Qasrawi AF, Gasanly NM. Semicond Sci Technol 2004;19:505.
[37] Kamal MM, Bhuiyan AH. Adv Mater Res 2013;741:59.
[38] Kim Y, Ohmi S, Tsutsui K, Iwai H. Jpn J Appl Phys 2005;44:4032.
[39] Sze SM, Ng KK. Physics of semiconductor devices. 3rd ed. New York: Wiley; 2006.
[40] Petkov P, Parvanov S, Petkova T. J Optoelect Adv Mater 2006;8(2):785.
[41] Lampert MA, Mark P. Current injection in solids. New York: Academic Press; 1970.
[42] Shukla P, Gaur MS. J Appl Polym Sci 2009;114:222.
[43] El-Nahass MM, Farid AM, Attia AA, Ali HAM. Egypt J Solids 2005;28:217.
[44] Anthopoulos TD, Shafai TS. Phys Stat Sol (a) 2000;181:569.